energies

MDPI

Article

Optimizing Alkaline Water Electrolysis: A Dual-Model Approach for Enhanced Hydrogen Production Efficiency

Simin Luo [1], Tengfei Zhang [2], Hongning Xu [2], Jie Zhang [2], Haichao Zhao [1], Jimmy Yun [1,*] and Hong Zhao [2,*]

[1] Qingdao Xinde New Energy Ltd., Qingdao 266021, China; luosimin0824@163.com (S.L.); zhaohaichao@xindeh2go.com (H.Z.)
[2] College of Chemical Engineer, Beijing University of Chemical Technology, Beijing 100029, China; wxyztf1116@163.com (T.Z.); 2019400041@mail.buct.edu.cn (H.X.); zhangjie@mail.buct.edu.cn (J.Z.)
* Correspondence: jimmy.yun@unsw.edu.au (J.Y.); 13693022763@163.com (H.Z.)

Abstract: This study develops a semi-empirical model of an alkaline water electrolyzer (AWE) based on thermodynamic and electrochemical principles to investigate cell voltage behavior during electrolysis. By importing polarization curve test data under specific operational conditions, eight undefined parameters are precisely fitted, demonstrating the model's high accuracy in describing the voltage characteristics of alkaline electrolyzers. Additionally, an AWE system model is introduced to examine the influence of various operational parameters on system efficiency. This innovative approach not only provides detailed insights into the operational dynamics of AWE systems but also offers a valuable tool for optimizing performance and enhancing efficiency, advancing the understanding and optimization of AWE technologies.

Keywords: alkaline electrolysis; efficiency optimization; simulation analysis; hydrogen energy

1. Introduction

Renewable energy is crucial for mitigating environmental pollution and achieving sustainable development. With the expansion of renewable energy capacity, a stable and reliable method for energy storage and supply is urgently needed to overcome the fluctuating power output from renewable energy sources [1]. Coupling water electrolyzers with renewable energy sources is considered a promising approach for achieving long-period energy storage [2]. Hydrogen, generated via water electrolysis, offers the advantages of ease of transportation and storage as an energy carrier. Furthermore, it finds extensive applications across diverse sectors, including the chemical industry, metallurgy, and transportation, due to its versatile utility [3–9].

Based on the electrolytes employed, water electrolysis technology is classified into three distinct types: alkaline water electrolysis (AWE), proton exchange membrane water electrolysis (PEMWE), and solid oxide electrolysis cells (SOEC) [10–15]. Alkaline water electrolysis is recognized as a well-established technology. Due to its excellent reliability, security, and up to 15-year lifetime, AWE has wide commercial applications [2,16,17]. An AWE typically incorporates a dual-electrode system immersed in an aqueous electrolyte solution, consisting of either potassium hydroxide (KOH) or sodium hydroxide (NaOH), with the concentration maintained within the range of 25 to 30% [17–19]. These electrodes are segregated by a porous diaphragm [15,20,21]. Hydrogen is released from the cathode, and hydroxide anions pass through the porous diaphragm, forming water and oxygen at the anode surface. The reaction of alkaline water electrolysis is demonstrated below:

$$Cathode: \quad 2H_2O + 2e^- \rightarrow H_2 + 2OH^- \tag{1}$$

$$Anode: \quad 2OH^- \rightarrow H_2O + 0.5O_2 + 2e^- \tag{2}$$

$$Overall: \quad H_2O \rightarrow 0.5O_2 + H_2 \tag{3}$$

check for updates

Citation: Luo, S.; Zhang, T.; Xu, H.; Zhang, J.; Zhao, H.; Yun, J.; Zhao, H. Optimizing Alkaline Water Electrolysis: A Dual-Model Approach for Enhanced Hydrogen Production Efficiency. *Energies* **2024**, *17*, 5512. https://doi.org/10.3390/en17215512

Received: 16 October 2024
Revised: 28 October 2024
Accepted: 31 October 2024
Published: 4 November 2024

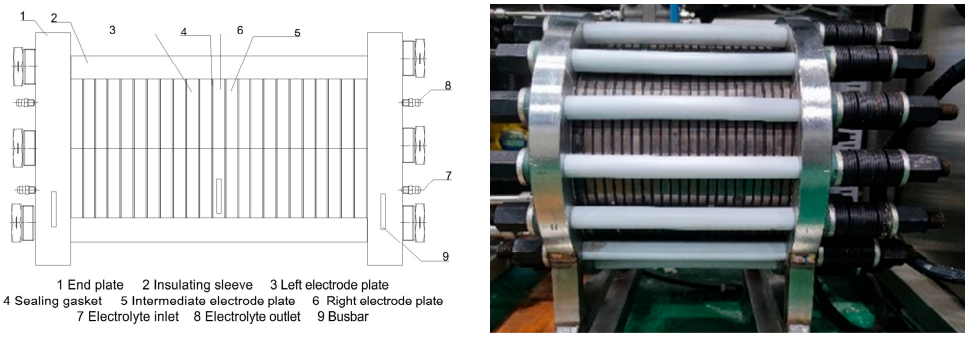
Copyright: © 2024 by the authors. Licensee MDPI, Basel, Switzerland. This article is an open access article distributed under the terms and conditions of the Creative Commons Attribution (CC BY) license (https://creativecommons.org/licenses/by/4.0/).

The process of alkaline water electrolysis encompasses electrode reactions, ion/proton transitions, thermodynamics, mass and heat transfer theory, as well as electrochemical theory [22]. Therefore, electrolysis processing can be described as a function of various parameters, including temperature [14], cell voltage [10], current density [23], and pressure [24]. Many AWE models have been established based on these chemical and physical parameters to predict the behavior of AWE systems. Abdin et al. [25] designed a model based on the physical principles associated with the materials and configuration of its components. While offering improvements in catalyst and bubble management, Abdin's model, however, overlooks critical parameters, such as wettability factors, charge transfer coefficients, surface roughness factors, and baseline exchange current densities. Ulleberg [26] developed an empirical model, integrating multiple foundational theories to predict cell voltage, hydrogen production, and efficiencies. The accuracy of Ulleberg's empirical model was verified using a photovoltaic-hydrogen system. This model has played a positive role in the optimization of electrolyzer design and the development of advanced control strategies. However, temperature is the only variable considered in Ulleberg's model. Thus, subsequent research introduces more variables to improve the accuracy of the electrolysis model. Sánchez et al. [27] take pressure into account based on Ulleberg's model, which was verified by a 15 kW alkaline test bench.

Cell voltage is a crucial parameter for assessing the performance of an AWE system. It is influenced by several operating parameters, including operation temperature, pressure, and lye flows. Optimization of the AWE system can be achieved through adjustment of these parameters. In order to investigate the voltage behavior of an alkaline electrolyzer with a hydrogen production capacity of 2 Nm^3/h across a comprehensive range of operating parameters, the relationship between the electrolyzer's voltage and the current density is rigorously analyzed employing a modeling methodology. The polarization curve of an electrolytic cell, under specified conditions in an alkaline water electrolysis cell, is measured, and a nonlinear fitting is applied to determine unidentified parameters. Subsequently, the model facilitates exploration of the impacts of current density, temperature, and pressure on the cell's voltage behavior. Furthermore, this study also introduces an AWE model in Aspen Plus (V 8.4) for the analysis of current density, temperature, and pressure effects on the system's efficiency and power dynamics. The modeling of electrolytic cells and AWE systems lays a robust foundation for the strategic selection and design of various system components, thereby enhancing the academic discourse on optimization strategies for AWE systems.

2. Alkaline Electrolyzer Voltage Computational Methods

Figure 1a illustrates the schematic diagram of the alkaline water electrolyzer used in this study, highlighting key components, such as the end plates, electrode plates, insulating sleeves, sealing gaskets, electrolyte inlets and outlets, and the busbar. Figure 1b shows the AWE utilized in this research, and its parameters are shown in Table 1.



(**a**) (**b**)

Figure 1. (**a**) Schematic of the alkaline water electrolyzer stack and (**b**) picture of the alkaline water electrolyzer stack.

Table 1. Basic parameters of the alkaline electrolyzer.

Parameters	Value	Unit
Hydrogen production	2	Nm^3/h
Current	200	A
Effective reaction area	0.0333	m^2
Current density	6000	A/m^2
Cell number	24	Pcs
Operation temperature	85	°C
Operation pressure	1.6	MPa

The electrolytic cell is the basic structure of the AWE system, where the water electrolysis reaction occurs. The working surface area of the electrodes is a critical factor in evaluating the efficiency of the electrolysis process. Larger electrode surface areas are known to enhance electrolysis efficiency by providing more active sites for the electrochemical reactions, thereby reducing activation overpotentials and improving overall reaction kinetics [1,2]. The nickel-plated nickel mesh electrodes with surface activation treatment were specifically chosen to maximize the effective surface area. This increased surface area enhances the electrochemical reaction rate by providing more active sites for the electrolysis reactions, thereby reducing overpotential and improving overall electrolysis efficiency [10]. Additionally, the mesh structure of the electrodes helps in minimizing the inter-electrode gap, further contributing to the reduction of ohmic losses and enhancing the performance of the electrolyzer. Previous studies have demonstrated that increasing the surface area of electrodes can significantly improve hydrogen production rates in alkaline water electrolysis systems [28,29]. In this study, the type of electrode used in the alkaline electrolyzer was a nickel-plated nickel mesh with surface activation treatment. This material structure effectively reduces overpotential and improves the electrolysis efficiency due to its increased electrochemical reaction area, reduced inter-electrode gap, and overall compact structure. Additionally, mesh electrodes are easy to manufacture and convenient to assemble and maintain.

The choice of electrolyte, whether NaOH or KOH, significantly impacts the electrolysis efficiency due to differences in several key parameters. KOH solutions generally exhibit higher conductivity compared to NaOH solutions, primarily due to the higher ionic mobility of potassium ions (K^+) versus sodium ions (Na^+) [30]. This higher mobility facilitates more efficient ion transport, which is crucial for achieving high electrolysis efficiency. Additionally, KOH solutions tend to have lower viscosity than NaOH solutions at the same concentration, which aids in better ion transport and reduces concentration overpotentials [31]. The lower viscosity of KOH solutions further enhances the electrochemical efficiency by decreasing the energy consumption required for the electrolysis process. Although NaOH solutions are still effective, their higher viscosity and lower ionic mobility can lead to slightly lower electrochemical efficiency and higher energy consumption compared to KOH solutions [32,33]. These differences justify the preference for KOH in many industrial applications where maximum efficiency is desired.

In this experiment, the electrolyte used was a KOH solution. Alkaline electrolytes, such as KOH, are widely used in water electrolysis due to their excellent conductivity, chemical stability, and high ionic mobility. These characteristics enable KOH solutions to maintain stable electrolysis efficiency under high current densities and voltages. Additionally, the relatively low viscosity of KOH solutions facilitates ion transport, thereby increasing electrode reaction rates, reducing concentration overpotentials, and improving overall efficiency [30,31].

The viscosity of the electrolyte and the rate of diffusion of ions significantly impact the efficiency of the electrolysis process. Higher viscosity can impede ion transport, leading to increased concentration overpotentials and reduced efficiency. Conversely, lower viscosity, often achieved by increasing the temperature, improves ion mobility and enhances the electrolyzer performance. The rate of diffusion of ions is crucial for maintaining high

reaction rates at the electrode surfaces. Faster diffusion rates ensure efficient ion transport to the electrodes, facilitating the electrochemical reactions necessary for hydrogen production. Studies have shown that optimizing these parameters can significantly improve the electrolyzer efficiency. For instance, reducing electrolyte viscosity through temperature control enhances mass transport, while considering ionic diffusion rates in the design process can lead to more efficient electrolyzers [32,33].

2.1. Thermodynamic Model

At normal temperature and pressure (NTP; 25 °C and 101.325 kPa), liquid water can dissociate into hydrogen and oxygen, which is shown in Equation (3). The standard molar enthalpy change, the standard molar entropy change, and the standard molar Gibbs free energy change of the electrolytic reaction are presented, as follows:

$$\Delta_r H_m^\theta = 285.83\,\mathrm{KJ/mol} \tag{4}$$

$$\Delta_r S_m^\theta = 163.34\,\mathrm{KJ/mol{\cdot}K} \tag{5}$$

$$\Delta_r G_m^\theta = \Delta_r H_m^\theta - T{\cdot}\Delta_r S_m^\theta = 237.13\,\mathrm{KJ/mol} \tag{6}$$

Variation in the electrolytic voltage with temperature is shown in Figure 2. The thermoneutral and equilibrium voltage curves divide this diagram into three parts. The formulas of those curves are shown below, respectively:

$$E_{\Delta H} = \frac{\Delta H}{2F} \tag{7}$$

$$E_{\Delta G} = \frac{\Delta G}{2F} = \frac{\Delta H - T{\cdot}\Delta S}{2F} \tag{8}$$

where F is the Faraday constant.

The equilibrium voltage is the theoretical minimum voltage necessary for water electrolysis, while the thermoneutral voltage represents the actual minimum voltage required to facilitate the electrolysis process. In Zone 1 (below the equilibrium voltage in which the H_2 generation is impossible), the electrolysis processing cannot carry on, and the value of the theoretical minimum voltage can be calculated by Equations (6) and (8), which is 1.2297 V. In Zone 2 (endothermic reaction), which is delineated by the region between the equilibrium line and the thermoneutral line, the progression of electrolysis necessitates the provision of an external heat source. In Zone 3 (exothermic reaction), situated beyond the thermoneutral voltage, electrolysis occurs with the release of heat. The thermoneutral voltage can be calculated by Equations (4) and (6), which is 1.482 V [26,34]. Usually, the operating voltage of a commercial AWE is 1.8–2.4 V, which indicates the electrolysis would be an exothermic reaction [35,36].

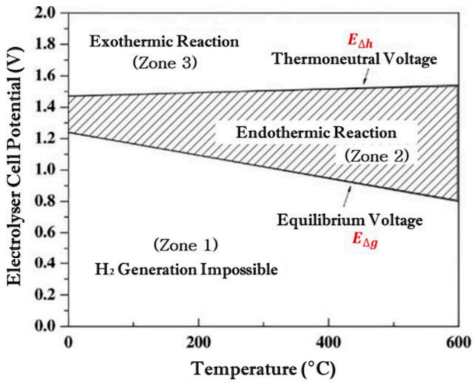


Figure 2. Change of electrolytic voltage with temperature [34].

2.2. Alkaline Electrolyzer Voltage Model

To accurately delineate the relationship between voltage and current within an electrolytic cell, a comprehensive consideration of thermodynamic, kinetic, and resistance-related effects is essential. During the electrolysis process, the observed voltage drop across the electrolysis cell is attributed to activation overpotential, ohmic overpotential, and concentration overpotential. In the typical operating range of an alkaline electrolyzer, the concentration overpotential is negligible, so the actual cell voltage can be expressed, as follows:

$$U_{cell} = E_{rev} + \eta_{ohm} + \eta_{act} \tag{9}$$

Here, U_{cell} is the cell voltage, E_{rev} is the reversible voltage, η_{ohm} is the ohmic overpotential, and η_{act} is the activation overpotential.

The reversible voltage can be calculated by Nernst equations:

$$E_{rev} = E^{\theta}_{rev}(T) + \frac{RT}{2F} In\left(\frac{\left(P - P_{lye}\right)^{1.5} \cdot P^{*}_{H_2O}}{P_{lye}}\right) \tag{10}$$

Here, P, T, R, and F are the operating pressure, temperature, universal gas constant, and Faraday constant, respectively. P_{lye} is the vapor pressure of KOH solutions, which is equal to the pressure of the wet hydrogen and oxygen gases near the electrode [14,37], and P_{H_2O} is the vapor pressure of water. The standard reversible potential varies as a function of temperature, and can be represented by the following empirical equation [37]:

$$E^{\theta}_{rev}(T) = 1.50342 - 9.956 \times 10^{-4} \times T + 2.5 \times 10^{-7} \times T^2 \tag{11}$$

Activation overpotential and ohmic overpotential are influenced by physical parameters, such as structure and material composition. Activation overpotential arises from the initiation of the water electrolysis reaction at the electrode surface. Conversely, ohmic overpotential is associated with the resistance encountered by the electrode, diaphragm, and electrolyte. Additionally, the formation of bubbles on the electrode surface also contributes to the ohmic overpotential [38]. Physical models can accurately predict the cell voltage behavior of electrolysis cells and study the influence of different parameters on cell voltage. However, some parameters are difficult to ensure, which inhibits the application of the physical model.

In this study, a semi-empirical model was developed to accurately delineate the polarization curve, with overpotential calculations based on empirical parameters. The construction of this model is underpinned by several foundational assumptions to affirm its accuracy: (1) The model presupposes a current efficiency of 100%, ignoring any secondary reactions during electrolysis to concentrate the analysis on the principal reactions. (2) It assumes the electrochemical properties across each electrolytic cell within an alkaline electrolyzer stack to be homogeneous, thereby guaranteeing uniform current and voltage throughout all cells—a crucial factor for the model's dependability. (3) It posits constant pressure and temperature conditions across all electrolytic cells, thereby providing a stable analytical framework. (4) It treats oxygen and hydrogen produced during electrolysis as ideal gases, which simplifies the calculations concerning gas behavior. (5) It disregards variations in the flow and temperature of the lye, focusing instead on the temperature of the lye at the inlet and outlet of the cell. This methodology obviates the need to consider dynamic shifts in lye conditions. By adopting these assumptions, the model is streamlined, reducing its complexity while preserving analytical accuracy, thus serving as an effective instrument for enhancing the efficiency of electrolysis processes.

The most representative semi-empirical model was developed by Ulleberg [26], which is based on thermodynamics and electrochemistry theory, using a nonlinear temperature function to describe the polarization curve of the electrolyzer. The formula is shown below:

$$U_{cell} = E_{rev} + \frac{r}{A} \cdot I + s \cdot ln(\frac{t}{A} \cdot I + 1) \quad (12)$$

Here, r is the parameter related to ohmic resistance, A is the area of the electrode (m^2), I is the current, and s and t are the coefficient for overvoltage on electrodes (V) and coefficient for overvoltage on electrodes (m^2/A), respectively, where r and t can be described as functions of temperature, and s is a constant [26]. So, Equation (12) can be modified as below:

$$U_{cell} = E_{rev} + (r_1 + r_2 \cdot T) \cdot i + s \cdot ln((t_1 + \frac{t_2}{T} + \frac{t_3}{T^2}) \cdot i + 1)) \quad (13)$$

Here, i is the current density (A/m^2). Ulleberg's model only takes temperature into account; thus, Sánchez et al. [27], based on Ulleberg's model, introduced parameter d into the model to improve the applicability. Here, d represents the variation in ohmic overpotential to pressure. The equation is shown below:

$$d = d_1 + d_2 \cdot p \quad (14)$$

Based on the above equations, the alkaline water electrolysis voltage can be expressed as:

$$\begin{aligned} U_{cell} = {} & 1.50342 - 9.956 \times 10^{-4} \times T + 2.5 \times 10^{-7} \times T^2 + \frac{RT}{2F} ln\left(\frac{(P - P_{lye})^{1.5} P_{H_2O}}{P_{lye}}\right) \\ & + [(r_1 + r_2 \cdot T) + (d_1 + d_2 \cdot P)] \cdot i + s \cdot ln\left[\left(t_1 + \frac{t_2}{T} + \frac{t_3}{T^2}\right) \cdot i + 1\right] \end{aligned} \quad (15)$$

Based on Equation (15), the electrolyzer model established in Simulink (V 7.0) is shown in Figure S1.

The relationship between the saturated vapor pressure of lye and pure water as a function of temperature was derived from Aspen Plus and imported into the Simulink model, as shown in Figure 3a,b, respectively. Both the lye and water saturated vapor pressure increased with the temperature rise.

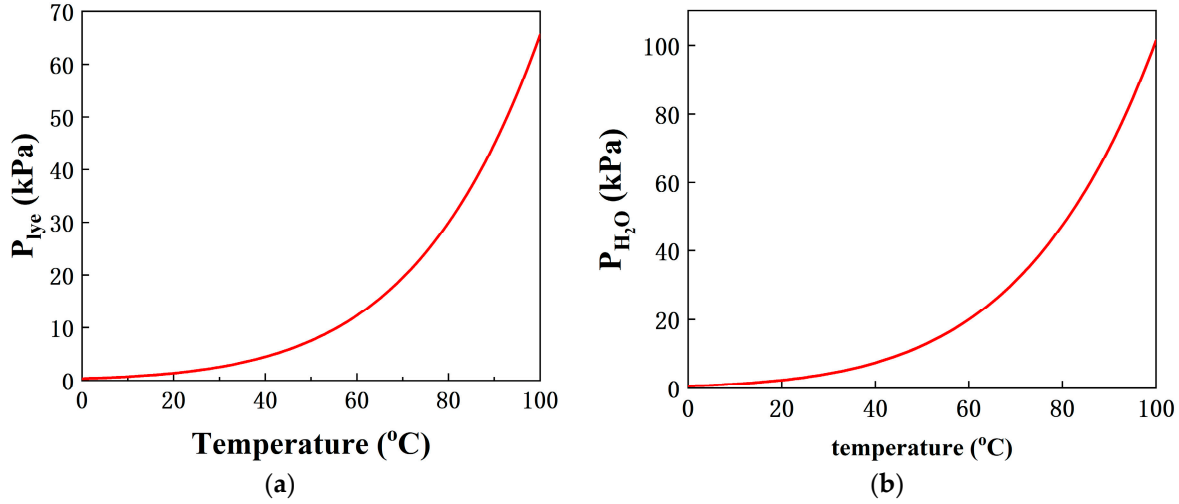


Figure 3. Saturated vapor pressure of (**a**) lye and (**b**) pure water changed with temperature.

3. Electrolyzer Model Validation and Parameter Analysis

3.1. Experimental Validation and Parameter Fitting for the Electrolyzer Model

Eight uncontained parameters in Equation (15) could be obtained from the experiment. Operating parameters are shown in Table 2.

Table 2. Operating parameters of the electrolyzer.

Parameters	Value
Inlet temperature (°C)	75
Outlet temperature (°C)	85
Operating pressure (MPa)	1.6
Lye flow (L/h)	280
Current density (A/m^2)	6000–1500 (decreases in steps of 500 A/m^2 until 1500 A/m^2)
Time (h)	2

Ten groups of data were obtained during the 2 h test: the first hour was spent waiting for the system to reach a stable state, and the other hour was spent collecting voltage data. The corresponding voltage value for each current density condition was the average voltage for the second hour. The test data are shown in Table 3.

Table 3. Electrolyzer polarization curve test data.

Current (A)	Voltage (V)	Current Density (A/m^2)	Cell Voltage (V)
199.97	50.89	6000	2.12
184.31	49.91	5500	2.08
166.65	49.21	5000	2.05
149.98	48.25	4500	2.01
134.32	47.03	4000	1.96
116.65	46.33	3500	1.93
99.99	45.11	3000	1.88
84.32	44.16	2500	1.84
66.66	42.97	2000	1.79
49.99	41.77	1500	1.74

Via nonlinear fitting of the data in Table 1, the values of eight unknown parameters could be determined, as shown in Table 4.

Table 4. Parameters' fitting values.

Parameters	Value	Unit
r1	4.825747×10^{-5}	$\Omega \cdot m^2$
r2	5.674751×10^{-8}	$\Omega \cdot m^2 \cdot °C^{-1}$
d1	6.230508×10^{-7}	$\Omega \cdot m^2$
d2	9.828342×10^{-7}	$\Omega \cdot m^2 \cdot bar^{-1}$
s	0.082272	V
t1	0.013255	$m^2 \cdot A^{-1}$
t2	4.151465	$m^2 \cdot °C \cdot A^{-1}$
t3	176.488351	$m^2 \cdot °C \cdot A^{-1}$

To validate the accuracy of the simulation result, the polarization curve of the electrolytic cell was measured under different inlet temperatures (75, 65, and 55 °C) and operating pressures (1.6, 1.3, and 1.0 MPa), with other parameters maintained. Those test results were compared with simulation results, and the determination coefficient, R2, was applied to identify the correlation between the test results and simulation results. R2 can be calculated as follows:

$$R^2 = 1 - \frac{\sum(X_{exp} - X_{sim})^2}{(N_{exp} - 1)\sum(X_{exp} - \overline{X})^2} \quad (16)$$

Figure 4a,b show the cell voltage variation under different operating pressures and temperatures. The determination coefficient under two different conditions was calculated,

and the average values were 99.94 and 99.82%, respectively. This indicated a good correlation between the measured values and simulation values, which means the as-established model could excellently reflect the cell voltage.

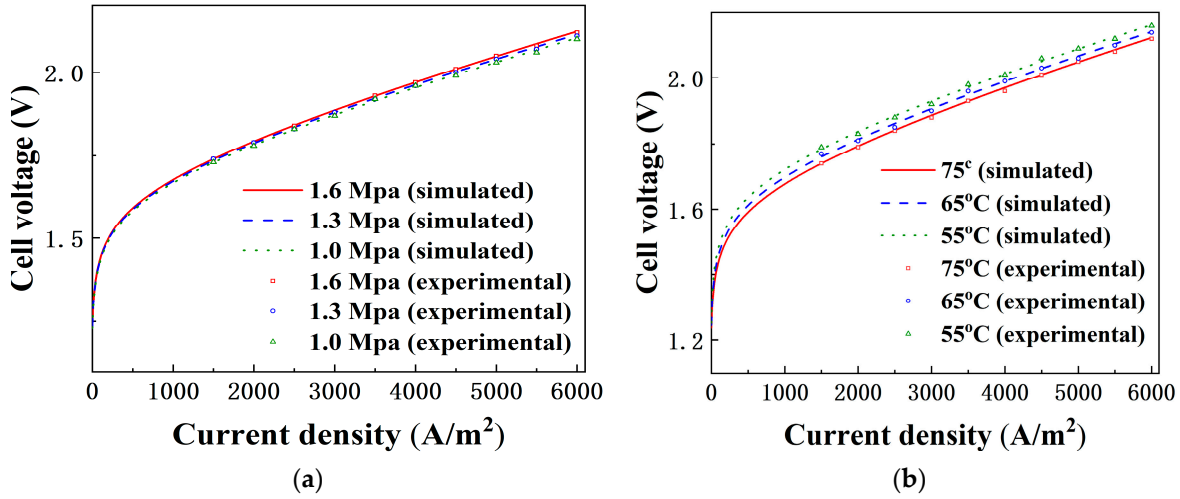


Figure 4. Comparison diagram between simulated and measured voltage values under different operating (**a**) pressures and (**b**) temperatures.

3.2. Analysis of Parameters Affecting Cell Voltage in an Alkaline Electrolyzer

After validation, we analyzed the effect of different parameters on the cell voltage, including current density, temperature, and pressure.

First, with the pressure and temperature maintained at stable levels, a simulation was conducted in the range from 0 to 12,000 A/m^2 to examine fluctuations in cell voltage, reversible voltage, ohmic overpotential, and activation overpotential. The results presented in Figure 5a demonstrate the variation in these variables as current density increased. As the current density increased, the cell voltage rose, particularly in the low current density region (0–1000 A/m^2). However, the reversible voltage remained constant. Additionally, both ohmic and activation potentials showed an increasing trend. Activation overpotential increased significantly in the low current density region, but the increase was not appreciable in the high current density region. On the other hand, ohmic overpotential exhibited a linear increase. The variation in activation overpotential explained the trend observed in the cell voltage variation. For this electrolyzer, a current density of 9380 A/m^2 represented a critical value. When the current density surpassed this limit, the activation overpotential exceeded the ohmic overpotential. In such instances, various strategies can be adopted to decrease the activation overpotential. For example, changing the electrode material to lower the activation energy barrier is one effective approach.

Additionally, the cell voltage of the alkaline electrolyzer was analyzed across a temperature range of 5–95 °C, under constant pressure, and over a current density range from 0 to 6000 A/m^2. The results depicted in Figure 5b show that the cell voltage gradually decreased with an increase in the temperature; specifically, the cell voltage dropped from 2.51 to 2.09 V as the temperature increased from 5 to 95 °C at a current density of 6000 A/m^2. To elucidate the impact of temperature on cell voltage, a simulation examining the relationship between variations in reversible voltage and overpotential was conducted. The outcomes of this simulation, illustrated in Figure 5c, indicated that both the reversible voltage and overpotential exhibited a gradual decline as the temperature increased. Notably, the decrease in reversible voltage was more pronounced than that observed in ohmic and activation overpotentials. The reduction in activation overpotential with rising temperature is a critical factor that accelerates electrolysis reactions. This is because higher temperatures can enhance the kinetics of the electrochemical reactions, thereby lowering the energy barrier for activation. Additionally, an increase in temperature also improves the conductivity of

the electrolyte, which contributes to a reduction in ohmic overpotential. Consequently, the thermal elevation plays a beneficial role in optimizing cell voltage by facilitating a more efficient transfer of ions across the electrolyte, further enhancing the overall efficiency of the electrolysis process. However, the benefits of higher temperatures come with the caveat of potential damage to the stability of the diaphragm within the electrolyzer. Elevated temperatures can adversely affect the mechanical and chemical stability of the diaphragm, leading to a diminished lifetime of the electrolyzer system. This presents a significant challenge, as the diaphragm's integrity is crucial for the effective separation of gases produced during electrolysis. Balancing the positive effects of temperature on electrolysis efficiency with the need to maintain the structural integrity of critical components, such as the diaphragm, is essential for the advancement and sustainability of electrolyzer technologies.

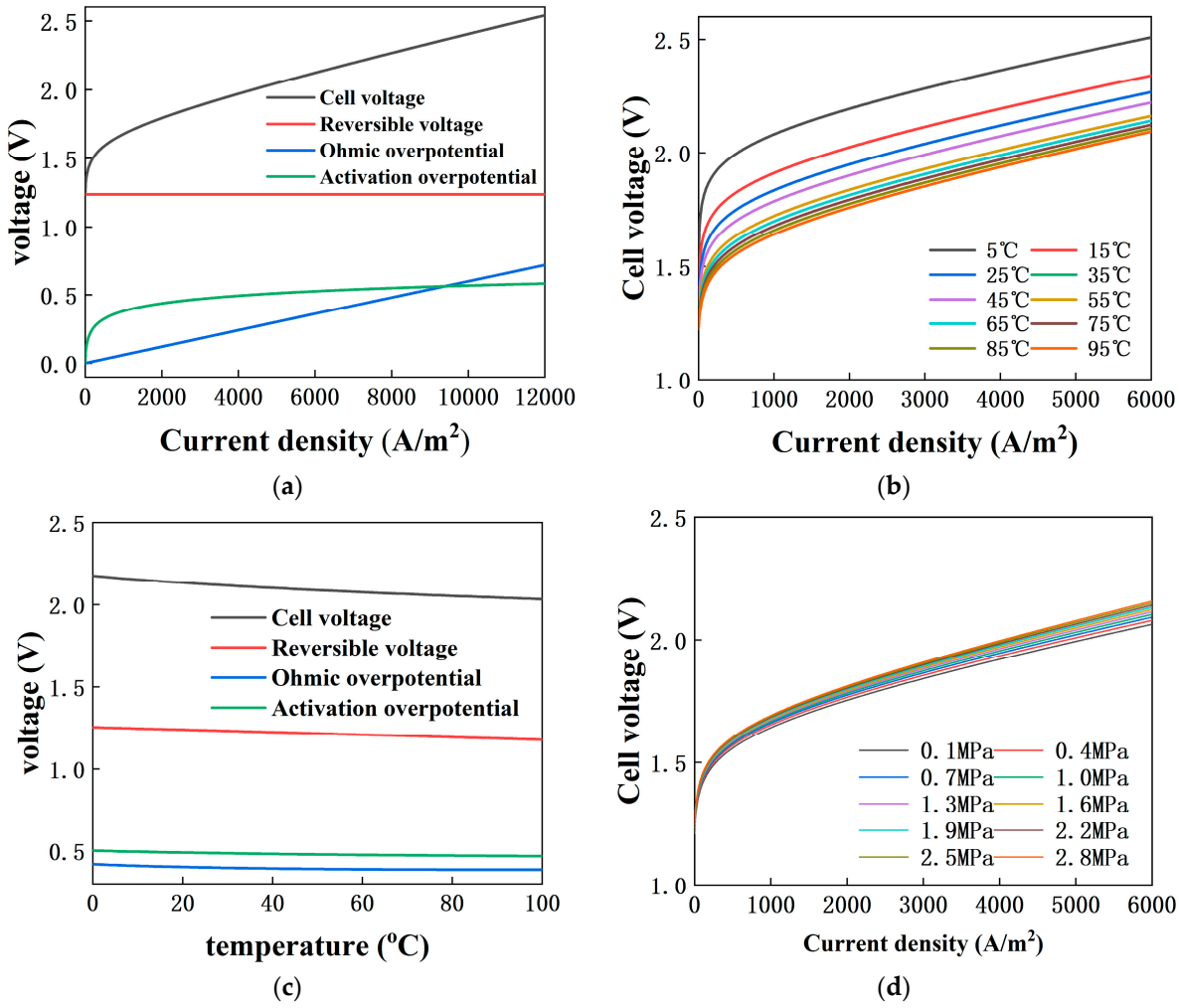


Figure 5. Variations in cell voltage, reverse voltage, ohmic overpotential, and activation overpotential against (**a**) current density and (**c**) temperature. Polarization curves of electrolytic cells under different (**b**) temperatures and (**d**) pressures.

Finally, the simulation of cell voltage in an alkaline electrolyzer across a pressure range from 0.1 to 2.8 MPa was conducted under constant temperature and within a current density range from 0 to 6000 A/m^2, as shown in Figure 5d. It was observed that, at a current density of 6000 A/m^2, the cell voltage experienced an increase from 2.06 to 2.16 V as the pressure rose from 0.1 to 2.8 MPa. According to Jang et al. [14], an increase in pressure led to a rise in reversible voltage, and both ohmic and activation overpotentials decreased as a consequence of diminished bubble coverage resulting from the increased pressure. Although the reversible voltage increased because of the elevated pressure—likely due

to the enhanced solubility of gases and improved reaction dynamics—the simultaneous decrease in overpotentials acted to moderate this effect. Consequently, these competing phenomena resulted in only a slight overall increase in cell voltage.

These investigations underscore the complex interplay of current density, temperature, and pressure in optimizing the electrolyzer performance, highlighting the need to balance these factors for enhanced efficiency and sustainability.

The semi-empirical model developed in this study provided valuable guidance for the practical selection of cathode and anode materials in alkaline water electrolyzers (AWEs). The model revealed the impacts of activation overpotential and ohmic overpotential on cell voltage during electrolysis and highlighted the regulatory effects of temperature and pressure on these overpotentials. When selecting cathode and anode materials, priority should be given to those that can reduce activation overpotential, such as nickel–molybdenum or nickel–iron alloys [28,29]. Additionally, materials with high electrical conductivity, such as nickel or stainless steel [39,40], should be chosen to minimize ohmic overpotential. The materials must also remain stable at the higher operational temperatures and pressures predicted by the model to achieve optimal performance. This decision-making process should balance the performance benefits with material costs, based on the simulation results from the model, to maximize electrolysis efficiency and optimize system performance.

4. Computational Method and Simulation-Based Analysis of Operational Parameter Impact on AWE System Efficiency

4.1. Model Description

During alkaline water electrolysis processing, about 70–90% of the input energy is used for electrolysis of water [41], while the rest is used to overcome internal resistance and convert into heat:

$$P = W + Q \tag{17}$$

Here, P is the input power, W is the electrolytic power, and Q is the thermal power, as follows:

$$P = n \cdot I \cdot E \tag{18}$$

$$W = n \cdot I \cdot E_{\Delta H} \tag{19}$$

$$Q = P - W \tag{20}$$

Here, E is the input voltage, $E_{\Delta H}$ is the equilibrium voltage, and n is the number of electrolyzer cells.

Thermal efficiency is a commonly used index to evaluate the electrolytic efficiency of an electrolytic cell. It is defined as the ratio of electrolytic power to the actual input power, which can equivalently be expressed as the ratio of equilibrium voltage to the actual electrolytic voltage [34], as shown below:

$$\eta = \frac{W}{P} = \frac{E_{\Delta H}}{E} \tag{21}$$

It is necessary to confirm $E_{\Delta H}$ to calculate the efficiency of the electrolysis system. Under NTP, the $E_{\Delta H}$ was 1.481 V, but the AWE system would not operate under these conditions. To confirm the $E_{\Delta H}$ under different operating parameters, an AWE system model was established in Aspen Plus to simulate the efficiency of the AWE system. The model is shown in Figure S2.

Figure S3 displays the parameter setting interface of the alkaline electrolyzer module. The AWE module calculated physical quantities, such as electric power and heat load, iteratively through parameters such as current and voltage. The voltage value was defined by using the design provisions found in Aspen process options, with efficiency from the input parameters serving as the control variable.

Via the simulation, the value of $E_{\Delta H}$ under different temperatures was obtained, which is indicated in Figure 6. The thermoneutral voltage declined as the operating temperature increased.

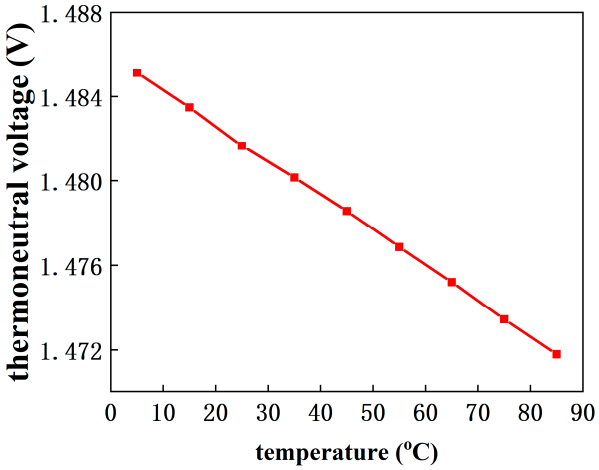


Figure 6. Thermoneutral voltage values at different reaction temperatures.

4.2. Simulation Influence of Operational Parameters on AWE System Efficiency

Based on the established model, we investigated how different parameters affected the efficiency of the alkaline water electrolysis (AWE) system.

Maintaining constant pressure and temperature, a simulation was conducted within a current density range from 500 to 6000 A/m^2 to examine the variations in thermal efficiency and electrolytic power, with the results depicted in Figure 7. As illustrated in Figure 7a, thermal efficiency declined from 93.65 to 70% as the current density increased from 500 to 6000 A/m^2. This trend suggests that higher current densities resulted in a significant decrease in thermal efficiency. Figure 8a further shows that with the increase in current density, there was a corresponding rise in input power, electrolytic power, and thermal power. However, it is crucial to note that the proportion of thermal power within the total input power increased, which negatively affected the thermal efficiency.

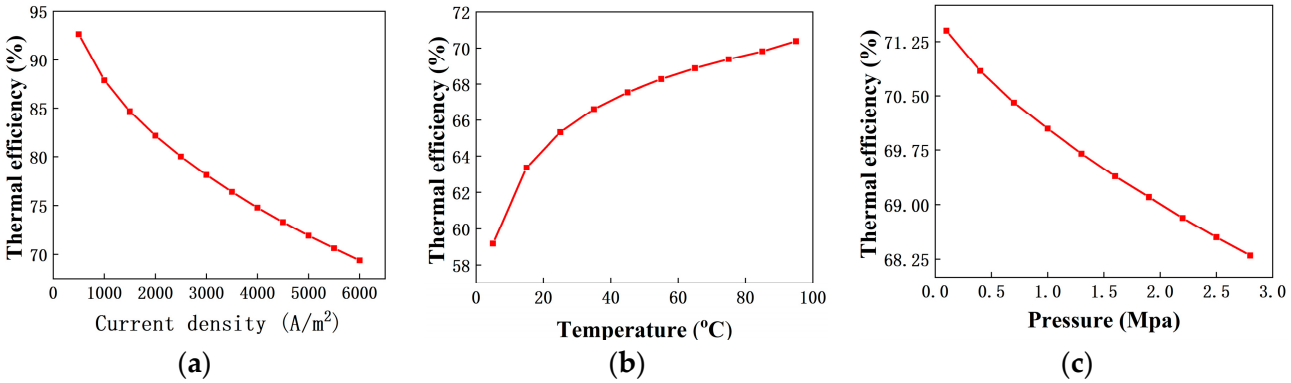


Figure 7. Variations in thermal efficiency under different (**a**) current densities, (**b**) temperatures, and (**c**) pressures.

To ensure consistent operating conditions, with both current density and pressure held constant, a simulation spanning a temperature range from 5 to 95 °C was performed. This investigation aimed to explore the fluctuations in thermal efficiency and electrolytic power, thereby providing insights into the temperature-dependent performance characteristics of the system. Figure 7b clearly demonstrates that thermal efficiency increased as the temperature rose. The increase in temperature created a more favorable environment for electrolysis by reducing the activation energy required for the electrochemical reactions,

thereby improving overall efficiency. However, Figure 8b shows that a notable consequence of this temperature increase was the elevated system heat production, which in turn raised the thermal load on the AWE system. This increase in thermal load necessitates effective heat management strategies to prevent any potential negative impacts on system components and to ensure the sustained high-efficiency operation of the AWE system.

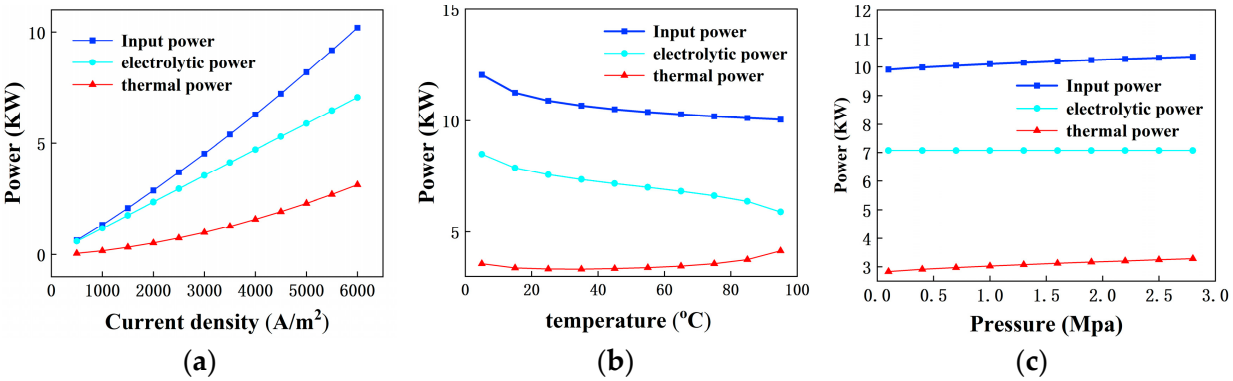


Figure 8. Variations in power under different (**a**) current densities, (**b**) temperatures, and (**c**) pressures.

With the operating current density and temperature held constant, a simulation was conducted across a pressure range of 0.1 to 2.8 MPa to examine the variations in thermal efficiency and electrolytic power. Figure 7c illustrates a decline in thermal efficiency concurrent with an increase in pressure, a phenomenon attributable to the escalation in thermal power depicted in Figure 8c. Meanwhile, both the input and electrolytic power exhibited negligible variations in response to the heightened pressure. This suggests that higher pressures in the AWE system could adversely affect its efficiency by elevating the thermal power, indicating an increase in energy lost as heat. Despite the increase in pressure, the stability of input and electrolytic power remained largely unaffected. However, the efficiency loss due to higher thermal power underlines the critical balance between the operating pressure and system performance. Therefore, operating the AWE system at elevated pressures could lead to diminished efficiency and increased energy consumption, highlighting the necessity of optimizing pressure settings to ensure energy-efficient and cost-effective hydrogen production.

The semi-empirical model developed in this study stands out from existing models by providing a more comprehensive and practical approach to the selection of electrode materials for alkaline water electrolyzers (AWEs). Unlike traditional models, which often narrowly focus on single factors, such as activation overpotential or ohmic overpotential, our model integrated these factors and considered the regulatory influences of temperature and pressure. This holistic approach enabled more precise predictions of cell voltage and efficiency under varying operational conditions. Additionally, the model's ability to guide the selection of materials that optimize both performance and cost represents a significant advancement. By incorporating practical considerations, our model offers a robust tool for designing more efficient and cost-effective electrolyzers, thereby pushing the boundaries of current electrolysis technology.

5. Conclusions

This study presented a comprehensive approach to modeling and analyzing an alkaline water electrolyzer (AWE) system using Simulink and Aspen Plus. The integration of these tools allowed for an in-depth examination of the factors influencing cell voltage and overall electrolysis efficiency. A semi-empirical voltage model based on thermodynamic and electrochemical principles was developed and validated using experimental data, achieving high accuracy, with determination coefficients (R^2) of 99.82% and 99.94%. The model considered critical operational parameters, including current density, temperature, and pressure, and their effects on cell voltage and system efficiency. Simulations revealed

that lower current densities significantly improved thermal efficiency, while elevated temperatures enhanced electrolysis efficiency but may compromise diaphragm stability. Increased pressure slightly raised the cell voltage due to the higher reversible voltage, despite the reduced overpotentials. The study also included a hydrothermal analysis of the AWE system, confirming the thermoneutral voltage at different operating temperatures. The findings underscore the importance of optimizing operational parameters to maximize energy efficiency and system performance. This dual-model approach not only enhances the understanding of AWE systems but also provides a valuable tool for optimizing their design and operation, promoting more efficient and sustainable hydrogen production.

Supplementary Materials: The following supporting information can be downloaded at: https://www.mdpi.com/article/10.3390/en17215512/s1, Figure S1: Voltage model of alkaline electrolyzer. Figure S2: Model of alkaline electrolyzer system. Figure S3: Electrolyzer Module Parameter Setting Interface.

Author Contributions: Conceptualization, S.L. and T.Z.; data curation, H.Z. (Haichao Zhao); formal analysis, T.Z. and H.Z. (Haichao Zhao); funding acquisition, J.Y.; investigation, T.Z. and H.Z. (Haichao Zhao); methodology, S.L. and T.Z.; project administration, H.Z. (Hong Zhao); resources, J.Y. and H.Z. (Hong Zhao); software, S.L. and H.X.; supervision, J.Z. and H.Z. (Hong Zhao); validation, H.X.; writing—original draft, S.L.; writing—review and editing, J.Z. and H.Z. (Hong Zhao). All authors have read and agreed to the published version of the manuscript.

Funding: This research received no external funding.

Data Availability Statement: The original contributions presented in the study are included in the article, further inquiries can be directed to the corresponding authors.

Conflicts of Interest: Authors Simin Luo, Haichao Zhao, Jimmy Yun were employed by the company Qingdao Xinde New Energy Ltd. The remaining authors declare that the research was conducted in the absence of any commercial or financial relationships that could be construed as a potential conflict of interest.

References

1. Haug, P.; Kreitz, B.; Koj, M.; Turek, T. Process Modelling of an Alkaline Water Electrolyzer. *Int. J. Hydrogen Energy* **2017**, *42*, 15689–15707. [CrossRef]
2. Gahleitner, G. Hydrogen from Renewable Electricity: An International Review of Power-to-Gas Pilot Plants for Stationary Applications. *Int. J. Hydrog. Energy* **2013**, *38*, 2039–2061. [CrossRef]
3. Jin, C.; Xiao, J.; Hou, J.; Jiang, H.; Zhang, J.; Lv, X.; Sun, W.; Jiang, H.; Du, E.; Fang, Y.; et al. Cross-Regional Electricity and Hydrogen Deployment Research Based on Coordinated Optimization: Towards Carbon Neutrality in China. *Energy Rep.* **2022**, *8*, 13900–13913. [CrossRef]
4. Shahabuddin, M.; Brooks, G.; Rhamdhani, M.A. Decarbonisation and Hydrogen Integration of Steel Industries: Recent Development, Challenges and Technoeconomic Analysis. *J. Clean. Prod.* **2023**, *395*, 136391. [CrossRef]
5. Shui, H.; Ge, R.; Zou, D.; Ren, S.; Li, Z.; Yan, J.; Lei, Z.; Wang, Z. Hydro-Refining of Coal-Petroleum Co-Processing Oil for Potential Clean Jet Fuels. *Fuel* **2022**, *323*, 124382. [CrossRef]
6. Manna, J.; Jha, P.; Sarkhel, R.; Banerjee, C.; Tripathi, A.K.; Nouni, M.R. Opportunities for Green Hydrogen Production in Petroleum Refining and Ammonia Synthesis Industries in India. *Int. J. Hydrogen Energy* **2021**, *46*, 38212–38231. [CrossRef]
7. Sollai, S.; Porcu, A.; Tola, V.; Ferrara, F.; Pettinau, A. Renewable Methanol Production from Green Hydrogen and Captured CO_2: A Techno-Economic Assessment. *J. CO_2 Util.* **2023**, *68*, 102345. [CrossRef]
8. Barreto, L.; Makihira, A.; Riahi, K. The Hydrogen Economy in the 21st Century: A Sustainable Development Scenario. *Int. J. Hydrogen Energy* **2003**, *28*, 267–284. [CrossRef]
9. Sebbahi, S.; Nabil, N.; Alaoui-Belghiti, A.; Laasri, S.; Rachidi, S.; Hajjaji, A. Assessment of the Three Most Developed Water Electrolysis Technologies: Alkaline Water Electrolysis, Proton Exchange Membrane and Solid-Oxide Electrolysis. *Mater. Today Proc.* **2022**, *66*, 140–145. [CrossRef]
10. Benghanem, M.; Almohamadi, H.; Haddad, S.; Mellit, A.; Chettibi, N. The Effect of Voltage and Electrode Types on Hydrogen Production Powered by Photovoltaic System Using Alkaline and PEM Electrolyzers. *Int. J. Hydrogen Energy* **2024**, *57*, 625–636. [CrossRef]
11. Grigoriev, S.A.; Porembsky, V.I.; Fateev, V.N. Pure Hydrogen Production by PEM Electrolysis for Hydrogen Energy. *Int. J. Hydrog. Energy* **2006**, *31*, 171–175. [CrossRef]

12. Lahrichi, A.; El Issmaeli, Y.; Kalanur, S.S.; Pollet, B.G. Advancements, Strategies, and Prospects of Solid Oxide Electrolysis Cells (SOECs): Towards Enhanced Performance and Large-Scale Sustainable Hydrogen Production. *J. Energy Chem.* **2024**, *94*, 688–715. [CrossRef]
13. Sumi, H. Co-Electrolysis SOEC and Internal Reforming SOFC for Achieving a Carbon-Neutral Society. *RSC Sustain.* **2024**, *2*, 1568–1579. [CrossRef]
14. Jang, D.; Cho, H.-S.; Kang, S. Numerical Modeling and Analysis of the Effect of Pressure on the Performance of an Alkaline Water Electrolysis System. *Appl. Energy* **2021**, *287*, 116554. [CrossRef]
15. Muhsen, H.; Alshawabkeh, M.; Al-Mahmodi, M.; Ghanem, A.; Al-Halhouli, A. Sensitivity Analysis of Electrodes Spacing Media for Evaluating Alkaline Electrolyzer Performance through CFD Modeling. *Renew. Energy Focus* **2024**, *49*, 100575. [CrossRef]
16. Sharshir, S.W.; Joseph, A.; Elsayad, M.M.; Tareemi, A.A.; Kandeal, A.W.; Elkadeem, M.R. A Review of Recent Advances in Alkaline Electrolyzer for Green Hydrogen Production: Performance Improvement and Applications. *Int. J. Hydrogen Energy* **2024**, *49*, 458–488. [CrossRef]
17. Volk, E.K.; Kreider, M.E.; Kwon, S.; Alia, S.M. Recent progress in understanding the catalyst layer in anion exchange membrane electrolyzers–durability, utilization, and integration. *EES Catal.* **2024**, *2*, 109–137. [CrossRef]
18. Martinez Lopez, V.A.; Ziar, H.; Haverkort, J.W.; Zeman, M.; Isabella, O. Dynamic Operation of Water Electrolyzers: A Review for Applications in Photovoltaic Systems Integration. *Renew. Sustain. Energy Rev.* **2023**, *182*, 113407. [CrossRef]
19. Sakas, G.; Ibáñez-Rioja, A.; Ruuskanen, V.; Kosonen, A.; Ahola, J.; Bergmann, O. Dynamic Energy and Mass Balance Model for an Industrial Alkaline Water Electrolyzer Plant Process. *Int. J. Hydrogen Energy* **2022**, *47*, 4328–4345. [CrossRef]
20. David, M.; Ocampo-Martínez, C.; Sánchez-Peña, R. Advances in Alkaline Water Electrolyzers: A Review. *J. Energy Storage* **2019**, *23*, 392–403. [CrossRef]
21. Lira Garcia Barros, R.; Kraakman, J.T.; Sebregts, C.; van der Schaaf, J.; de Groot, M.T. Impact of an Electrode-Diaphragm Gap on Diffusive Hydrogen Crossover in Alkaline Water Electrolysis. *Int. J. Hydrogen Energy* **2024**, *49*, 886–896. [CrossRef]
22. Cheng, H.; Xia, Y.; Hu, Z.; Xiong, J.; Wei, W. Modeling and Control for Alkaline Water Electrolyzers Operating in Wide Range. *IEEE Trans. Ind. Electron.* **2023**, *71*, 10888–10897. [CrossRef]
23. Zhang, D.; Zeng, K. Evaluating the Behavior of Electrolytic Gas Bubbles and Their Effect on the Cell Voltage in Alkaline Water Electrolysis. *Ind. Eng. Chem. Res.* **2012**, *51*, 13825–13832. [CrossRef]
24. Li, Y.; Zhang, T.; Ma, J.; Deng, X.; Gu, J.; Yang, F.; Ouyang, M. Study the Effect of Lye Flow Rate, Temperature, System Pressure and Different Current Density on Energy Consumption in Catalyst Test and 500W Commercial Alkaline Water Electrolysis. *Mater. Today Phys.* **2022**, *22*, 100606. [CrossRef]
25. Abdin, Z.; Webb, C.J.; Gray, E. MacA. Modelling and Simulation of an Alkaline Electrolyser Cell. *Energy* **2017**, *138*, 316–331. [CrossRef]
26. Ulleberg, Ø. Modeling of Advanced Alkaline Electrolyzers: A System Simulation Approach. *Int. J. Hydrogen Energy* **2003**, *28*, 21–33. [CrossRef]
27. Sánchez, M.; Amores, E.; Rodríguez, L.; Clemente-Jul, C. Semi-Empirical Model and Experimental Validation for the Performance Evaluation of a 15 kW Alkaline Water Electrolyzer. *Int. J. Hydrogen Energy* **2018**, *43*, 20332–20345. [CrossRef]
28. Song, S.; Zhang, H.; Ma, X.; Shao, Z. High-performance nickel-molybdenum electrocatalysts for hydrogen evolution reaction. *J. Power Sources* **2008**, *175*, 851–855. [CrossRef]
29. Xiang, D.; Bo, X.; Gao, X.; Zhang, C.; Du, C.; Zheng, F.; Zhuang, Z.; Li, P.; Zhu, L.; Chen, W. Novel one-step synthesis of core@shell iron–nickel alloy nanoparticles coated by carbon layers for efficient oxygen evolution reaction electrocatalysis. *J. Power Sources* **2019**, *438*, 226988. [CrossRef]
30. Hitchcock, L.B.; Mcilhenny, J.S. Viscosity and Density of Pure Alkaline Solutions and Their Mixtures. *ACS Publ.* **2002**, *27*, 461–466. [CrossRef]
31. Hammoudi, N.E.; Mai, T.H.; Savall, A. Mass Transport in Alkaline Electrolyzers: Ionic Diffusion and Conductivity. *Electrochim. Acta* **2011**, *59*, 539–546. [CrossRef]
32. Millet, P.; Ngameni, R.; Grigoriev, S.A.; Mbemba, N. Electrochemical performances of PEM water electrolysis cells and perspectives. *Int. J. Hydrogen Energy* **2011**, *36*, 4134–4142. [CrossRef]
33. Carmo, M.; Fritz, D.L.; Mergel, J.; Stolten, D. A comprehensive review on PEM water electrolysis. *Int. J. Hydrogen Energy* **2013**, *38*, 4901–4934. [CrossRef]
34. Zeng, K.; Zhang, D. Recent Progress in Alkaline Water Electrolysis for Hydrogen Production and Applications. *Prog. Energy Combust. Sci.* **2010**, *36*, 307–326. [CrossRef]
35. Zhou, H.; Yu, F.; Zhu, Q.; Sun, J.; Qin, F.; Yu, L.; Bao, J.; Yu, Y.; Chen, S.; Ren, Z. Water Splitting by Electrolysis at High Current Densities under 1.6 Volts. *Energy Environ. Sci.* **2018**, *11*, 2858–2864. [CrossRef]
36. Jeddizahed, J.; Webley, P.A.; Hughes, T.J. Integrating Alkaline Electrolysis with Oxyfuel Combustion for Hydrogen and Electricity Production. *Appl. Energy* **2024**, *361*, 122856. [CrossRef]
37. Hammoudi, M.; Henao, C.; Agbossou, K.; Dubé, Y.; Doumbia, M.L. New Multi-Physics Approach for Modelling and Design of Alkaline Electrolyzers. *Int. J. Hydrogen Energy* **2012**, *37*, 13895–13913. [CrossRef]
38. LeRoy, R.L.; Bowen, C.T.; LeRoy, D.J. The Thermodynamics of Aqueous Water Electrolysis. *J. Electrochem. Soc.* **1980**, *127*, 1954. [CrossRef]
39. Lasia, A. *Electrochemical Impedance Spectroscopy and Its Applications*; Springer Nature: Berlin/Heidelberg, Germany, 2019. [CrossRef]

40. Lavorante, M.J.; Franco, J.I. Performance of stainless steel 316L electrodes with modified surface to be use in alkaline water electrolyzers. *Int. J. Hydrogen Energy* **2016**, *41*, 9731–9737. [CrossRef]
41. Koponen, J. Review of Water Electrolysis Technologies and Design of Renewable Hydrogen Production Systems. Veden elektrolyysiteknologiat ja uusiutuvan vedyn tuotantojärjestelmien suunnittelu. 2015. Available online: https://lutpub.lut.fi/bitstream/handle/10024/104326/MScThesis_JKK.pdf;jsessionid=766AE469B1D21717071F16DC7CF3F7E3?sequence=2 (accessed on 30 October 2024).

Disclaimer/Publisher's Note: The statements, opinions and data contained in all publications are solely those of the individual author(s) and contributor(s) and not of MDPI and/or the editor(s). MDPI and/or the editor(s) disclaim responsibility for any injury to people or property resulting from any ideas, methods, instructions or products referred to in the content.